1   **Epigenetic regulation of genome integrity by a prion-based mechanism**
2
3   James S. Byers[1], David M. Garcia[2], and Daniel F. Jarosz[1,2,]*
4
5
6
7
8
9
10
11
12
13
14
15
16
17
18
19
20
21
22
23
24
25
26
27
28
29
30
31
32
33
34
35
36
37
38
39
40   **Affiliations:**
41
42   [1]Department of Developmental Biology, Stanford University School of Medicine, 269 Campus Drive,
43   Stanford, CA 94305
44
45   [2]Department of Chemical and Systems Biology, Stanford University School of Medicine, 269 Campus
46   Drive, Stanford, CA 94305
47
48   *To whom correspondence should be addressed: jarosz@stanford.edu

49   **ABSTRACT**

50

51   Epigenetic mechanisms mediate diverse gene expression programs in growth and development. Yet

52   whether any can permanently alter the genome is unknown. Here we report a protein-based epigenetic

53   element, a prion, formed by the conserved DNA helicase Mph1/FANCM. [$MPH1^+$] provides resistance to

54   DNA damage, a gain-of-function trait that requires helicase activity and interactions with other DNA

55   repair proteins. Strikingly, the intrinsically disordered regions of Mph1 and human FANCM that are

56   required for prion phenotypes do not resemble known prions. [$MPH1^+$] reduces mitotic mutation rates,

57   but promotes meiotic crossovers, driving phenotypic diversification in wild outcrosses. Remarkably,

58   [$MPH1^+$] is induced by stresses in which the prion is beneficial. Thus, [$MPH1^+$] fuels a quasi-Lamarckian

59   form of inheritance that promotes survival of the current generation and diversification of the next.

60

INTRODUCTION

61

62 All organisms must faithfully transmit a genetic blueprint comprising ~10^6 to ~10^9 base pairs to the next

63 generation. This challenge is met by an ancient cohort of proteins that orchestrate error-free replication

64 and DNA repair (Whitby, 2010). Many such activities are organized by a helicase known as Mph1

65 (mutator phenotype 1) in fungi and FANCM (Fanconi Anemia complementation group M) in animals and

66 plants (Crismani et al., 2012; Moldovan and D'Andrea, 2009). Mph1/FANCM also drives diverse

67 biochemical activities including DNA-dependent ATPase function, replication fork reversal, and D loop

68 dissociation (Whitby, 2010). In humans, mutations in FANCM are associated with Bloom's syndrome and

69 elevated cancer rates, underscoring its central importance in ensuring genome integrity (Alter, 1996;

70 Meetei et al., 2003). A hallmark of Fanconi anemia patients is extreme sensitivity to chemotherapeutics

71 that create DNA inter-strand crosslinks or double strand breaks (DSBs) (Moldovan and D'Andrea, 2009).

72 In nature DSBs arise commonly during sexual reproduction, where they serve as intermediates for

73 meiotic recombination, but vastly exceed the number of crossovers in most organisms (McMahill et al.,

74 2007). Recent studies in *Arabidopsis thaliana* and *Schizosaccharomyces pombe* suggest that, by

75 suppressing crossover events, Mph1/FANCM provides a molecular explanation for this imbalance

76 (Crismani et al., 2012; Lorenz et al., 2012).

77 Here we report that Mph1 has the capacity to act as protein-based epigenetic element, a prion,

78 that we term [*MPH1*$^+$] (brackets denote non-Mendelian meiotic segregation; capitalization denotes

79 dominance). [*MPH1*$^+$] is adaptive during genotoxic stress. It also exerts a strong influence on genome

80 fidelity, decreasing mutagenesis in mitotic growth while increasing the frequency with which DSBs are

81 resolved as crossovers during sexual reproduction. [*MPH1*$^+$] can be induced by the same stresses to

82 which it provides resistance, providing a molecular mechanism for quasi-Lamarckian inheritance. Our

83 data thus establish [*MPH1*$^+$] as an inducible epigenetic state that simultaneously guards the genome

84   against insult during mitotic division and promotes its permanent and heritable diversification during

85   meiosis.

86

87   **Methods**

88   **Yeast Techniques.** Yeast strains (Table S1) were obtained from stock centers or generously provided by

89   the sources indicated. All strains were stored as glycerol stocks at −80 °C and revived on YPD before

90   testing. Yeast were grown in YPD at 30 °C unless indicated otherwise. Yeast transformation was

91   performed with a standard lithium–acetate protocol (Gietz et al., 1992).

92   For yeast crossing experiments, MATa and MATα mating types each lacking a unique

93   auxotrophic marker were mixed overnight in YPD. This mixture was then plated on plates selecting for

94   these 2 auxotrophies to select for diploids (usually minus lysine and minus methionine). After 3 days,

95   colonies were picked and grown in 8 mLs pre-sporulation media (8 g Yeast Extract, 3 g Bacto Peptone,

96   100 g Dextrose, 100 mg adenine sulfate per liter) overnight. The next morning, the cells were washed

97   and resuspended in 3 mLs sporulation media (10 g potassium acetate, 1 g yeast extract, 0.5 g glucose,

98   0.1 g amino acid add-back per liter). Cells were incubated for 7 days at room temperature and spores

99   were enriched as described previously (Rockmill et al., 1991).

100   Cytoduction experiments were performed as described previously (Chakrabortee et al., 2016).

101   Briefly, initial BY4742 recipient strains generated by transformation introducing a defective KAR allele

102   (*kar1-15*) that prevents nuclear fusion during mating (Wickner et al., 2006). Strains were made 'petite'

103   (incompetent for mitochondrial respiration) by inoculating a single colony in YPD with 0.25% ethidium

104   bromide and growing culture at 30 °C until late exponential/stationary phase (OD_{600} ~ 1). Cultures were

105   diluted 1:1000 into fresh YPD with ethidium bromide and the previous steps were repeated twice.

106   Cultures were plated to single colonies and multiple were tested for respiration incompetence (i.e. no

107   growth on YP-Glycerol). For initial cytoduction into BY4742**,** donor BY4741 strains harboring [*MPH1*$^+$]

108   and naïve BY4742 *kar1-15* recipient strains were mixed on the surface of a YPD agar plate. These were

109   grown for 24 hours and transferred to media lacking methionine and containing glycerol as a carbon

110   source (SGly-MET). This selects for both BY4742 nuclear markers along with restoration of functional

111   mitochondria via cytoplasmic exchange. After 3-5 days, multiple single colonies were picked and

112   passaged with another round of selection on SD-MET. In parallel, these colonies were confirmed to be

113   haploid by passage on SD-LYS-MET medium. For reverse cytoductions, the new donor strains (this time

114   the successful BY4742 *kar1-15* cytoductants) were mixed with petite naïve BY4741 cells (generated as

115   above) on YPD agar. Cytoductions were repeated as described previously except selecting for BY4741

116   recipient nuclear markers on glycerol media lacking lysine (SGly-LYS). Multiple cytoductants were picked

117   and tested for the presence of [*MPH1*$^+$] phenotypes.

118

119   **Phenotypic assays.** Biological replicates of each yeast strain (BY4741 MATa haploids) were pre-grown in

120   rich media (YPD). We then diluted these saturated cultures 1:10 in sterile water and then inoculated 1.5

121   μL into 96-well plates with 150 μL of YPD (SD-CSM was used instead with cisplatin and mitomycin C) per

122   well with the following stressors: phleomycin 5μg/mL; mycophenolic Acid – 20 μM; hydroxyurea – 400

123   mM; 4-nitroquinoline 1-oxide – 1.2 μM; cisplatin – 8 mM; methyl methanesulfonate – 0.012%;

124   camptothecin –50 μM; doxorubicin – 80 μM; oxolinic acid – 100 μM; mitomycin C – 1mM. We grew cells

125   at 30 °C in humidified chambers for 96 h and continuously measured growth by OD$_{600}$ in a microplate

126   reader. Timepoints plotted in bar graphs correspond to the point of greatest difference between [*mph1*$^-$

127   ] and [*MPH1*$^+$]: phleomycin – 1225 min; mycophenolic Acid – 755 min; hydroxyurea – 2500 min; 4-

128   nitroquinoline 1-oxide – 2500 min; methyl methanesulfonate – 1600 min; camptothecin – 900 min;

129   doxorubicin – 2000 min; oxolinic acid – 755 min; mitomycin C – 2500 min.

130   For genetic interaction experiments, phenotyping was performed similarly to before but instead

131   in 384-well plates to generate additional technical replicates for each strain. Briefly, biological replicates

132   of each knockout were pre-grown in rich media (YPD) in 96-well plates. We did not analyze mutants of

133   two additional interacting proteins, Rfa1 and Smc5, which were associated with strong sporulation

134   defects unrelated to the prion (Farmer et al., 2011; Soustelle et al., 2002)). We then diluted these

135   saturated cultures 1:10 in sterile water and then inoculated 5 µL in a 1:4 array into 384-well plates with

136   45 µL of YPD+4-NQO per well. However, because each genetic knockout was differentially sensitive to

137   genotoxic stress, different concentrations of the chemical were used for each genotype: *rad5Δ* − 2 µM;

138   *rad51Δ* − 1.5 µM; *sgs1Δ* − 1 µM; *srs2Δ* − 2 µM; *mhf1Δ* − 1.5 µM; *mhf2Δ* − 2 µM; *chl1Δ* − 2 µM; *exo1Δ* −

139   1.5 µM; *mgm101Δ* − 1 µM; *msh2Δ* − 1 µM; *msh6Δ* − 2 µM; *pso2Δ* − 1.5 µM; *slx4Δ* − 2 µM. We grew cells

140   at 30 °C in humidified chambers for 96 h and continuously measured growth by OD_{600} in a microplate

141   reader. The Log2 fold-change values plotted correspond to the highest OD_{600} value reached for each

142   strain (i.e. the carrying capacity). The same concentrations were used for the phenotyping of the

143   corresponding heterozygous, cross-back diploids.

144

145   **Microscopy**. Microscopy was performed using a Leica inverted fluorescence microscope with a

146   Hammamatsu Orca 4.0 camera. Cells were imaged after growth to exponential phase (OD600 of 0.7) or

147   stationary phase (OD 1.5 or above after 2 days) in a medium that minimizes autofluorescence (per liter

148   in water: 6.7 g yeast nitrogen base without ammonium sulfate, 5 g casamino acids, 20 g glucose).

149   Exposure time was 2 seconds.

150

151   **Protein Transformation**. Lysate transformations were performed as described previously (Chakrabortee

152   et al., 2016; Tanaka and Weissman, 2006). Briefly, 50 mL cultures of [$MPH1^+$] strains were grown in YPD

153   for 18 h, pelleted, washed twice with H_2O and 1 M sorbitol respectively, and then resuspended in 200 µL

154   of SCE buffer (1 M sorbitol, 10 mM EDTA, 10 mM DTT, 100mM sodium citrate, 1 Roche mini-EDTA-free

155   protease inhibitor tablet per 50 mL, pH 5.8) containing 50 units/mL of zymolyase 100T. Cells were

156   incubated for 30 min at 35°C, sonicated on ice for 10 s with a sonic dismembrator at 20% intensity, and

157   cell debris was removed via centrifugation at 10,000g at 4°C X 15 min. Supernatants were digested with

158   3-fold excess RNAse I and biotinylated DNAse (as determined by units of activity) (Thermo AM1906) for

159   1 h at 37°C. DNase was subsequently removed by adding saturating quantities of streptavidin-sepharose

160   beads, incubating for 5 min, and bead pelleting via centrifugation (this allows addition of a *URA3*-

161   marked plasmid for selection later). Nuclease digested supernatants were used to transform naïve

162   recipient yeast spheroplasts. Cells were harvested as before, re-suspended in 200 U/mL zymolyase 100T

163   in 1 M sorbitol, and incubated at 35°C for 15 min. Spheroplasts were collected by centrifugation, and

164   washed twice with 1 mL sorbitol and 1 mL STC buffer (1 M sorbitol, 10 mM $CaCl_2$, 10 mM Tris pH 7.5)

165   respectively, and re-suspended in STC buffer using wide-mouthed pipet tips to avoid lysis. Aliquots of

166   spheroplasts were transformed with 50 μL of lysate, 20 μL salmon sperm DNA (2 mg/mL), and 5 μL of a

167   carrier plasmid (*URA3*- and GFP-expressing pAG426-GFP). Spheroplasts were incubated in

168   transformation mix for 30 min at room temperature, collected via centrifugation, and resuspended in

169   150 μL of SOS-buffer (1 M sorbitol, 7 mM $CaCl_2$, 0.25% yeast extract, 0.5% bacto-peptone). Spheroplasts

170   were recovered at 30°C for 30 min and the entire culture was plated on SD-URA plates and overlaid with

171   warm SD-CSM containing 0.8% agar. After 2-3 days, dozens of Ura+ colonies were picked and re-

172   streaked on SD-URA selective media. The carrier plasmid was subsequently removed by section on 5-

173   FOA and single colonies were tested for the transmission of [*MPH1*^{+}]-dependent phenotypes. Infectivity

174   is calculated as percent of transmission divided by the amount of seeded protein used (estimate 77

175   molecules/cell of Mph1) (Kulak et al., 2014).

176

177   **Mutagenesis assays.** Yeast strains were grown in multiple biological replicates to saturation in YPD.

178   Then 1 mL was spun down, resuspended in 100 μL H_2O, and plated on SD-Arg (6.7 g yeast nitrogen base

179   without ammonium sulfate, 5 g casamino acids without arginine, 20 g glucose per liter) + 60 μg/mL

7

180   Canavanine (forward mutagenesis), YPD + 100 μM Fluconazole, or 60 μg/mL Canavanine and 1 g/L 5-

181   Fluoroorotic acid (GCR mutagenesis). Plates were incubated for 3 days and then CFUs were counted

182   using a colony counter (Synbiosis Acolyte).

183

184   **Induced mutagenesis and prion switching assays.** Yeast strains (BY4741 or *MDG1::K.lactisURA3*

185   reporter strains) were grown with 3 biological replicates to saturation in YPD with the indicated

186   chemicals for induced mutagenesis frequencies (0.012% MMS, 100 μM Oxolinic Acid) or for [*MPH1$^+$*]

187   reporter switching (2.4 μM 4-NQO, 400 μM Camptothecin, 2 mM Cisplatin, 0.024% H$_2$O$_2$, 400 mM

188   Hydroxyurea, 0.012% MMS). For starvation conditions in [*MPH1$^+$*] reporter switching, yeast strains were

189   grown with 3 biological replicates to saturation in YPD and then washed once with water and

190   resuspended in the following media conditions (no glucose, nitrogen limitation, phosphate limitation,

191   and sporulation media). Then 1 mL was spun down, resuspended in 100 μL H$_2$O, and plated on the

192   indicated selective plates: SD-Arg (6.7 g yeast nitrogen base without ammonium sulfate, 5 g casamino

193   acids without arginine, 20 g glucose per liter) + 60 μg/mL Canavanine (forward mutagenesis) or SD-URA

194   (50 mg uracil, 6.7 g yeast nitrogen base without ammonium sulfate, 5 g casamino acids, 20 g glucose per

195   liter) + 1 g/L 5-FOA (reporter switching). Plates were incubated for 3 days and then CFUs were counted

196   using a colony counter (Synbiosis Acolyte). For prion reporter switching, *MDG1* has no defined function

197   in mutagenesis or DNA repair, but is down-regulated in [*MPH1$^+$*] cells. Thus, [*mph1$^-$*] cells can grow on

198   media lacking uracil, but [*MPH1$^+$*] cells cannot. In contrast, [*MPH1$^+$*] cells can grow on 5-FOA, whereas

199   [*mph1$^-$*] cells cannot.

200

201   **Meiotic Recombination Assays.** Meiotic reporter strains were generated by amplifying a *K.lactis URA3*

202   cassette off the *pUG72* plasmid (Euroscarf) with primers targeting the marker 50kb upstream of the

203   *his3Δ* locus of BY4741. These PCR products were transformed into [*mph1$^-$*], [*MPH1$^+$*], and *mph1Δ* strains

204   as described above. A functional *HIS3* marker was also re-integrated back into its endogenous locus via

205   PCR into *BY4742* [*mph1*⁻] wild-type and *mph1Δ. BY4741* and *BY4742* strains of the corresponding *MPH1*

206   genotype were crossed to generate His+ Ura+ diploids and then sporulated as described above. Dozens

207   of colonies were picked for each and tested for co-segregation of *URA3* and *HIS3* markers.

208   For the genetic cross experiments with lab and clinical strains, the [*mph1*⁻] and [*MPH1*⁺]

209   laboratory strains above were crossed to the clinical isolate YJM975 (SGRP). Diploids were sporulated as

210   before and then 96 spores were picked for each. Spores were pinned in quadruplicate onto solid YPD

211   plates with the follower stressors: 39°C, 128 µg/mL fluconazole, 1 mM amphotericin B, 120 µg/mL

212   calcofluor white, 0.01% H_2O_2. Yeast were grown at 30°C (except in the case of 39°C heat stress) for 3-4

213   days and then pictures were taken and colony size analysis was conducted using SGAtools (Wagih et al.,

214   2013). Distributions were normalized to the means of the population.

215

216

217

218

219

220

221

222

223

224

225

226

227

228   **RESULTS**

229   **[*MPH1⁺*] is a protein-based genetic element**

230   We previously found that transient overexpression of Mph1 could elicit heritable zinc resistance that

231   had properties consistent with protein-based inheritance (Chakrabortee et al., 2016). These included

232   non-Mendelian segregation of this phenotype in genetic crosses (it was inherited by all meiotic progeny

233   rather than half), and a strong reliance on molecular chaperones (Hsp70 proteins) for propagation from

234   one generation to the next. This chaperone dependence was unusual – most previously known prions

235   depend on Hsp104 to propagate (Shorter and Lindquist, 2005) – and Mph1 lacks the glutamine or

236   asparagine-rich regions typical of nearly all known prions. We therefore investigated whether this

237   Mph1-dependent epigenetic state was a *bona fide* protein-based genetic element.

238   Prion acquisition commonly elicits heritable changes in the localization of causal protein(s)

239   (Derkatch et al., 2001). We investigated whether this was true for the Mph1-dependent epigenetic

240   state, taking advantage of the fact that prions are dominant (Shorter and Lindquist, 2005). We crossed a

241   yeast strain expressing an endogenous *MPH1-YFP* fusion to a strain harboring the Mph1-dependent

242   epigenetic state, and to genetically identical (isogenic) naïve cells as a control. There was no apparent

243   difference between these groups in exponentially growing cells. However, in stationary phase cells,

244   Mph1-YFP foci were evident in diploids harboring the Mph1-dependent epigenetic state, but not in

245   isogenic naïve diploids (Fig. S1).

246   We next tested whether the Mph1-dependent epigenetic state could be transmitted by

247   cytoplasmic mixing without transfer of any nuclear material, another hallmark of prion biology (Wickner

248   et al., 2006). To do so, we performed 'cytoduction' experiments with *kar1-15* mutants in which nuclei do

249   not fuse during mating (Fig. S2A; see methods). The Mph1-dependent epigenetic state was robustly

250   transferred to naïve recipient cells through such 'cytoduction' experiments (Fig. S2B). These data thus

251   establish that the phenotype did not arise from genetic mutation.

10

252   Finally, we performed a protein transformation as the 'gold-standard' test for prion-based

253   inheritance. We generated nuclease-digested lysates from cells harboring the Mph1-dependent

254   epigenetic state and from isogenic naïve cells. We used these lysates to transform naïve spheroplasts

255   (yeast lacking a cell wall), including a carrier plasmid harboring a *URA3* marker to enrich for cells that

256   were competent to uptake molecules from their external milieu (Fig. S2C; see methods). We picked

257   dozens of Ura+ colonies, propagated them on 5-FOA to select for loss of the carrier plasmid, and

258   characterized the phenotypes of the resulting cells. Strikingly, over 40% of them also acquired the

259   Mph1-dependent epigenetic state (scored by resistance to $ZnSO_4$; Fig. 1A; $p=1.6 \times 10^{-4}$ by t-test). When

260   benchmarked against the low natural abundance of Mph1 (~80 molecules per cell (Kulak et al., 2014)),

261   this frequency of transmission is substantially more efficient than for other prions that have been tested

262   (Tanaka and Weissman, 2006). We conclude that the Mph1-dependent epigenetic state is a *bona fide*

263   protein-based genetic element – a prion – which we hereafter refer to as [*MPH1*$^+$].

264

265   **[*MPH1*$^+$] promotes DNA damage tolerance and genome stability**

266   Because Mph1 plays a central role in genome integrity we tested the ability of [*MPH1*$^+$] cells to

267   withstand DNA damage. The prion had no effect on growth in rich medium alone. We next exposed

268   [*mph1*$^-$], [*MPH1*$^+$], and *mph1*Δ cells to a battery of genotoxic insults, including replication stressors

269   (hydroxyurea, mycophenolic acid), intercalating agents (doxorubicin), lesion inducers (4-NQO), alkylating

270   agents (MMS), topoisomerase inhibitors (oxolinic acid), DNA break inducers (phleomycin), and

271   crosslinkers (cisplatin, camptothecin, mitomycin C). In most of these conditions, cells harboring [*MPH1*$^+$]

272   grew better than isogenic [*mph1*$^-$] cells, and the prion was never maladaptive (Fig. 1B). In contrast,

273   *mph1*Δ cells were hypersensitive to most genotoxic stressors. Many amyloid-based prions act by

274   sequestering their constituent protein into aggregates. Thus their phenotypes often mimic the

275   corresponding genetic loss-of-function. Our data indicate that [*MPH1*+] is capable of driving gain-of-

276   function phenotypes.

277   Mph1 overexpression strongly increases the frequency of gross chromosomal rearrangements

278   (GCR) and, conversely, *mph1Δ* decreases GCR formation (Banerjee et al., 2008). We observed no

279   influence of [*MPH1*+] on GCRs using the same reporter strains employed in those studies (*p*=0.40 by

280   Student's t-test, Fig. S3) however, establishing that the prion state is distinct from a simple increase in

281   Mph1 activity. We also examined mutagenesis using an assay in which loss-of-function mutations in the

282   *CAN1* gene render cells resistant to the toxic arginine analog canavanine. As others have reported

283   (Scheller et al., 2000), *mph1Δ* cells had an approximately tenfold increased spontaneous mutagenesis

284   frequency compared to wild-type cells. In contrast, [*MPH1*+] cells had a three-fold *decreased* frequency

285   of spontaneous mutation compared to isogenic [*mph1*-] cells (Fig. 1C), again consistent with [*MPH1*+]

286   driving gains-of-function. We observed the same anti-mutator phenotype when scoring resistance to the

287   antifungal drug fluconazole (Fig. 1D), establishing that these relationships were not unique to the

288   forward mutagenesis assay employed. We also observed decreased frequencies of induced mutagenesis

289   in [*MPH1*+] cells (e.g. with MMS and oxolinic acid; Fig. 1C).

290   One possible explanation for the decreased mutation frequency in [*MPH1*+] cells would be

291   preferential engagement of error-free repair pathways, which often involve homologous recombination.

292   Indeed, Mph1 has been implicated in pathway choice decisions in multiple organisms (Huang et al.,

293   2013; Xue et al., 2015b) and [*MPH1*+] provides resistance to agents that induce DSBs (*e.g.* phleomycin;

294   Fig. 1B), which serve as precursors to HR. Using a simple assay for integration of a *HIS3* marker at its

295   endogenous locus (see methods), we found that [*MPH1*+] drives a robust increase in HR (5.3-fold;

296   *p*=0.003 by t-test; Fig. S4), providing a possible explanation for the reduced mutagenesis frequency.

297   Collectively, our data establish that [*MPH1*+] enhances survival and preserves genome integrity during

298   wide range of genotoxic insults.

299

[*MPH1*^{+}] phenotypes require helicase function

The gains-of-function in [*MPH1*^{+}] cells led us to investigate whether Mph1's catalytic activity was required for prion-dependent phenotypes. To test this, we employed a well-characterized inactivating point mutation in Mph1's active site (*mph1-Q603D*, (Chen et al., 2009)). We crossed isogenic [*MPH1*^{+}] and [*mph1*[-]] cells to a naïve strain harboring *mph1-Q603D*, selected diploids, sporulated them, and then examined meiotic progeny that harbored the *mph1-Q603D* alleles (Fig. 2A).

As expected, [*MPH1*^{+}] progeny harboring the wild-type allele were more resistant to 4-NQO than matched [*mph1*[-]] progeny (*p*=0.014 by t-test, Fig. 2B). In contrast, [*MPH1*^{+}] progeny harboring the *mph1-Q603D* allele were as sensitive to 4-NQO as [*mph1*[-]] progeny harboring the catalytically inactive variant (*p*=0.21, Fig. 2B). Thus, Mph1 activity is required to produce [*MPH1*^{+}] phenotypes. We tested whether Mph1 catalytic function was also required for prion propagation (Fig. 2A). To do so we crossed meiotic progeny (arising from the previous cross) harboring the *mph1-Q603D* allele to naïve, wild-type strains to create heterozygous diploids in which Mph1 function was restored. Prion-dependent resistance to 4-NQO re-emerged in these strains (*p*= 0.047 by t-test, Fig. 2B), establishing that the helicase function of Mph1 is required to produce DNA damage resistance, but not to propagate the prion itself.

315

[*MPH1*^{+}] phenotypes require FA pathway components

As a scaffold, Mph1 interacts with many factors involved in both error-free and error-prone DNA repair (Daee et al., 2012; Ward et al., 2012; Xue et al., 2015a). We applied classical epistasis to examine how these interactions influence [*MPH1*^{+}]-dependent phenotypes, capitalizing on the fact that [*MPH1*^{+}] is transmitted to all progeny of meiosis (Chakrabortee et al., 2016). We crossed isogenic [*MPH1*^{+}] and [*mph1*[-]] cells to naïve strains harboring deletions of thirteen previously reported Mph1-interacting genes, related helicases, proteins involved in inter-strand crosslink (ICL) repair, and FA pathway

13

323   components. We then sporulated these diploids and selected six [*MPH1*⁺] and [*mph1*⁻] progeny

324   harboring each gene deletion. Finally, we exposed these strains to genotoxic stress and compared how

325   [*MPH1*⁺] affected survival in the context of each gene deletion.

326   We observed strong genetic interactions between [*MPH1*⁺] and components of the FA pathway.

327   This network has been best characterized in the context of ICL repair, where Mph1 scaffolds

328   Msh2/Msh6 to recruit Exo1 and digest the ICL-harboring oligonucleotide. Mhf1/Mhf2 stabilizes Mph1

329   complexes on chromatin at stalled replication forks and Chl1 (the yeast FancJ homolog) and Slx4 (the

330   yeast FancP homolog) mediate downstream gap re-filling and fork reset (Daee et al., 2012). Loss of each

331   of these FA factors eliminated [*MPH1*⁺]-dependent resistance to genotoxic stress (Fig. 2C).

332   Deletion of two genes encoding proteins related to Mph1/ICL repair, Pso2 (a nuclease and

333   member of an orthogonal ICL epistasis group) (Ward et al., 2012) and Srs2 (the yeast RTEL1 helicase

334   homolog), abolished the [*MPH1*⁺] phenotype, even though they are not linked to the FA pathway (Daee

335   et al., 2012). These epistasis patterns establish that the phenotypic effects of [*MPH1*⁺] require

336   engagement of most yeast Fanconi proteins (Ward et al., 2012), as well as other factors that are thought

337   to function in independent, parallel repair pathways (Fig. 2C), raising the possibility that [*MPH1*⁺] exerts

338   its phenotypes by re-wiring crosstalk among DNA repair factors.

339   We next tested whether these Mph1 interactions were required for prion propagation. To do so

340   we crossed the haploid deletion strains in which [*MPH1*⁺]-dependent phenotypes had disappeared to

341   naïve wild-type strains, creating heterozygous diploids in which gene function was restored. Strikingly,

342   resistance to genotoxic stress re-emerged in only 3 strains: *exo1Δ/EXO1*, *rad5Δ/RAD5*, and

343   *mgm101Δ/MGM101* (Fig. 2C). Thus, the remaining proteins (Rad51, Srs2, Mhf1, Mhf2, Chl1, Msh2,

344   Msh6, Pso2, Slx4), which include most of the FA pathway, are required not only to manifest [*MPH1*⁺]

345   phenotypes, but also to propagate the prion.

346   Genetic requirements for mutagenesis and survival in DNA damage can differ. We therefore

14

347   investigated how the loss of these same genes affected the anti-mutator phenotype of [*MPH1*⁺]. (This

348   was only possible in haploids because most canavanine resistant mutants are recessive.) Cells lacking

349   Mgm101, Pso2, and Rad51 inherited anti-mutator phenotypes from an [*MPH1*⁺] parent (Table S3), but

350   those lacking Rad5, Msh2, Msh6, or Mhf1 did not inherit an anti-mutator phenotype. Strikingly, [*MPH1*⁺]

351   led to large *increases* in mutation frequency in strains lacking Slx4 and Mhf2. Mhf2 stabilizes aberrant

352   DNA structures, allowing helicases such as Mph1 to remodel them. Slx4 is a structure-specific

353   endonuclease that also acts on aberrant DNA structures (particularly branched substrates) (Fricke and

354   Brill, 2003). Slx4 has overlapping specificity with another DNA helicase, Sgs1 (BLM in humans), which

355   interacts with topoisomerase 3 to process stalled replication forks (Fricke and Brill, 2003). As with Slx4,

356   loss of Sgs1 also led to a strong mutator phenotype in the presence of [*MPH1*⁺]. Our data thus strongly

357   suggest that the anti-mutator phenotype in [*MPH1*⁺] cells depends on Slx4, Sgs1, and Mhf2 activities,

358   and likely their ability to resolve aberrant DNA intermediates in a non-mutagenic fashion.

359

360   **Prion-dependent toxicity of Mph1 and FANCM overexpression**

361   A hallmark of many prion proteins is that they can be toxic when overexpressed in matched [*PRION*⁺]

362   strains, but not in naïve cells (Fig. 3A). This toxicity typically requires specific protein domains that are

363   important for prion propagation (Douglas et al., 2008). Mph1 overexpression from a constitutive

364   promoter was indeed significantly more toxic in [*MPH1*⁺] cells than in [*mph1*⁻] cells (*p*=0.04 by t-test, Fig.

365   3B). We used this growth impairment as a tool to dissect which domains of Mph1 fuel its prion-like

366   properties. Mph1 does not harbor N/Q-rich prion-like domains (Fig. 3C). However, it does contain

367   multiple, large, extremely disordered regions outside of its helicase domain (Jones and Cozzetto, 2015)

368   (Fig. 3D), particularly at the C-terminus. This pattern of disorder is highly conserved in the human

369   ortholog FANCM (Fig. 3D), and truncation of the disordered C-terminal region is the most frequent

370   FANCM variant observed in human cancers (Cerami et al., 2012). Notably, Mph1 variants lacking its large

371   C-terminal disordered region did not exert prion dependent toxicity (Fig. 3B), despite similar levels of

372   expression (Fig. S5), establishing the importance of this disordered region in prion-dependent

373   phenotypes.

374   We also transformed [$mph1^-$] cells and [$MPH1^+$] cells with plasmids encoding full-length FANCM

375   and a variant lacking its disordered C-terminus (FANCMΔC) under the control of the same constitutive

376   promoter. Expression of full-length FANCM was also more toxic in [$MPH1^+$] cells than in isogenic [$mph1^-$]

377   cells (p=0.036 by t-test, Fig. 3B). In contrast, FANCMΔC did not affect growth of either [$mph1^-$] or

378   [$MPH1^+$] cells (p=0.47 by t-test, Fig. 3B). Thus, despite its limited sequence identity, human FANCM

379   appears to interact with yeast [$MPH1^+$] to exert a toxicity that depends upon both its disordered C-

380   terminus and the presence of the prion.

381

382   **Induction by environmental stress**

383   It has been suggested that prions might drive a quasi-Lamarckian form of inheritance (Halfmann et al.,

384   2010; True and Lindquist, 2000), fueling heritable and adaptive phenotypic changes in response to

385   transient environmental stressors (Holmes et al., 2013). Many prions can be modestly induced by

386   perturbations that disrupt protein homeostasis (Jarosz et al., 2010). Yet only two, [GAR^+] (Jarosz et al.,

387   2014) and [MOD^+] (Suzuki et al., 2012), are known to be induced by the same stresses to which they

388   provide resistance. We tested whether any of the DNA damaging stresses in which [$MPH1^+$] provides a

389   benefit might also elicit its appearance, as would be expected for a Lamarckian epigenetic element. We

390   did so using an $MDG1$::$URA3$ reporter that we previously established provides a readout of the [$MPH1^+$]

391   prion state (Chakrabortee et al., 2016) (Fig. 4A).

392   Exposure to hydroxyurea increased the frequency of [$MPH1^+$] acquisition seven-fold in these

393   experiments (p=0.035 by t-test; Fig. 4B). We observed no such effect for many other DNA damaging

394   agents in which [$MPH1^+$] provides an equivalent or greater adaptive advantage. These data establish

16

395   that the increased frequency of [*MPH1⁺*] did not merely arise from selection for the prion. Starvation for

396   another nutrient, phosphate, also strongly induced [*MPH1⁺*] (6.4-fold, p=0.041 by t-test). Both

397   hydroxyurea and phosphate starvation have been linked to replication stress via depletion of

398   deoxynucleotide pools (Young et al., 1967). Thus, [*MPH1⁺*] can be induced not just by overexpression, as

399   we did artificially, but also by a specific replication stressor to which it provides resistance, establishing

400   that this prion can act as a quasi-Lamarckian element of inheritance.

401   Because replication stresses acted as a trigger for [*MPH1⁺*], we wondered whether intermediate

402   structures in DNA repair processes might be important for templating and/or propagating the prion.

403   Mph1 binds to specific DNA fork structures to assemble larger complexes at sites of damage (Xue et al.,

404   2015b). Furthermore, other types of nucleic acids have been hypothesized to act as scaffolds for prion-

405   like aggregation in amyloid bodies (Audas et al., 2016). Constitutive overexpression of Mph1 also leads

406   to a mutator phenotype (Banerjee et al., 2008) that depends upon inactivation of another specialized

407   DNA helicase, Pif1, which efficiently unwinds a type of DNA secondary structure known as G-

408   quadruplexes (Paeschke et al., 2013). These guanine repeats form a stable planar structure through

409   hydrogen bonding, which impedes their traversal by the replication machinery. We *transiently*

410   overexpressed *PIF1* for ~25 generations in [*MPH1⁺*] and [*mph1⁻*] cells and investigated whether they

411   maintained [*MPH1⁺*]-dependent decreases in mutagenesis. Immediately following *PIF1* overexpression,

412   [*MPH1⁺*]-dependent decreases in mutagenesis were completely abolished (*p*=0.40 by t-test, Fig. 4C.).

413   However, after we removed the *PIF1* plasmid and propagated the strains 3 times on standard rich

414   medium (YPD) the [*MPH1⁺*]-dependent mutagenic phenotypes re-emerged (*p*=0.027 by t-test, Fig. 4C).

415   These results indicate that specific DNA structures, such as G-quadruplex regions or perhaps other Pif1

416   substrates, may play a central role in the manifestation of the [*MPH1⁺*] phenotype, but are not required

417   for propagation of the prion.

418

17

419 **[*MPH1*⁺] increases genetic and phenotypic diversification during meiosis**

420 Experiments in *Arabidopsis thaliana* (Crismani et al., 2012) and *Schizosaccaromyces pombe* (Lorenz et

421 al., 2012) have identified Mph1/FANCM as the strongest known inhibitor of crossover formation during

422 meiosis. We therefore tested whether [*MPH1*⁺] exerted any influence on meiotic crossovers in *S.*

423 *cerevisiae*. To do so we constructed a yeast strain harboring a functional *URA3* cassette 50kb upstream

424 of a non-functional *his3Δ1* mutation, enabling us to examine co-segregation of these linked genetic

425 markers (Fig. 5A). We mated this strain, which could grow on media lacking uracil but not on media

426 lacking histidine, to isogenic [*MPH1*⁺] and [*mph1*⁻] strains, which harbored a non-functional *ura3Δ0*, but

427 an intact *HIS3* locus. We then selected diploids and induced meiosis. There was no difference in

428 sporulation efficiency between [*mph1*⁻] and [*MPH1*⁺] harboring cells (*p*=0.45 by Student's t-test, Fig. S6).

429 After 10 days, we isolated meiotic progeny and examined the frequency of His+ Ura+ recombinant

430 spores derived from both [*MPH1*⁺] and [*mph1*⁻] parents. Recombinant phenotypes (*i.e.* those in which

431 re-assortment of linked parental markers occurred) were substantially more common in meiotic

432 progeny derived from [*MPH1*⁺] parents compared to those derived from [*mph1*⁻] parents (4.4-fold; *P* =

433 0.02 by T-test; Fig. 5B), establishing that the prion fundamentally altered the degree of linkage the cross.

434 *S. cerevisiae* naturally produces many crossovers per chromosome, a feature that has motivated

435 its use as a genetic model organism. As a consequence, its linkage blocks are small and most

436 polymorphisms within them are thought to be passenger mutations rather than causal variants. We

437 nonetheless investigated whether [*MPH1*⁺] might spark increased phenotypic variation in natural *S.*

438 *cerevisiae* outcrosses. We mated isogenic [*mph1*⁻] and [*MPH1*⁺] laboratory strains to a sequenced clinical

439 strain isolated from an Italian patient (YJM975 (Strope et al., 2015)). As a frame of reference, the genetic

440 divergence between open reading frames in these strains (0.5%) is only slightly greater than that

441 between human individuals. We isolated diploids from these matings, induced meiosis, and isolated

442 spores (Fig. 5C; see SI). We confirmed that these spores were *bona fide* meiotic recombinants based on

18

443   mating type tests and then exposed these progeny to physiological stressors relevant to the clinical

444   niche: heat stress, antifungal drugs, and oxidative stress, measuring colony size as a proxy for growth.

445   The presence of [*MPH1*$^+$] significantly increased the phenotypic variation in these cells (Fig. 5D-G).

446   To test whether this increased phenotypic diversity arose from the enhanced re-assortment of

447   genetic information during meiosis, or rather due to some other effect of [*MPH1*$^+$] (*e.g.* decreased

448   mutation rate, phenotypic capacitance, etc.), we also examined phenotypic variation produced by the

449   prion in the parental strains. We transferred [*MPH1*$^+$] to each parent by cytoduction (see SI for

450   experimental details) and examined the variance in phenotype across the same stressors that we used

451   to examine the meiotic progeny. The variance in phenotype imparted by [*MPH1*$^+$] was much smaller in

452   each parent than it was in the meiotic progeny (Fig. 5D-G, Fig. S7) and curing of the prion did not

453   eliminate these traits (Fig. S9), establishing that the prion itself did not increase phenotypic variance in a

454   static genetic background. Thus, even given a restricted degree of parental genetic diversity and the high

455   baseline recombination rate of *S. cerevisiae*, [*MPH1*$^+$] can sharply increase heritable phenotypic

456   diversification during meiosis.

457   Changes in protein homeostasis have previously been shown to modulate genotype to

458   phenotype relationships (Jarosz et al., 2010). To confirm that [*MPH1*$^+$] was not acting as a phenotypic

459   capacitor and influencing manifestation of the observed phenotypes in the new genetic backgrounds,

460   we picked multiple meiotic progeny and "cured" them of [*MPH1*$^+$] via transient inhibition of the

461   molecular chaperone Hsp70 (Chakrabortee et al., 2016). Outlier progeny both resistant and sensitive to

462   heat stress were transformed with a plasmid containing a dominant negative variant of Hsp70 (Ssa1-

463   K69M) and propagated for ~75 generations on selective media to eliminate inheritance of the prion (as

464   has been described previously). Then the plasmid was eliminated and normal Hsp70 function was

465   restored for an additional ~25 generations. The strains were then arrayed onto a plate in a 10-fold

466   dilution series and allowed to grow up for 3 days (Fig. S8). While [*MPH1*$^+$]-dependent phenotypes (e.g.

467   zinc resistance) were curable in this experiment, phenotypes that arose uniquely in the meiotic progeny

468   (e.g. resistance to heat stress) were not.

469

470
471
472

Discussion

To survive in dynamic, fluctuating environments, organisms must acquire new heritable traits. However, a multitude of mechanisms that safeguard DNA replication often create a phenotypic 'lock in', limiting the source of biological novelty to relatively modest changes in the genetic code. Dynamic, environmentally regulated signaling networks offer one solution to this problem. Epigenetic 'bet-hedging' mechanisms may provide another (Halfmann et al., 2010; Lancaster and Masel, 2009; True and Lindquist, 2000). Such systems increase phenotypic variation, creating sub-populations that express different traits than the majority. In fluctuating environments, these new traits might enable survival of the population when it would otherwise have perished. However, the evolutionary value of most bet-hedging systems, including those driven by prions, depends upon the constant presence of the causal element. Mechanisms of this type have been implicated in the interpretation of genetic information (True and Lindquist, 2000), but none are known to permanently alter the genome. Our data establish that one such element, the prion [$MPH1^+$], has the power to do so. This prion is highly transmissible and can be induced in environments where it is adaptive, providing a robust mechanism for Lamarckian inheritance that controls fundamental decisions in DNA damage tolerance, mutagenesis, and meiotic recombination.

Perhaps the greatest force driving genetic diversification in eukaryotes is sexual reproduction. Re-assortment of alleles in meiosis ensures that every genome is fundamentally new. But within this genomic patchwork, linkage blocks can be found in which multiple polymorphisms are inherited in *cis*. As an epistemological tool, geneticists have long assumed that individual, 'driver' polymorphisms are linked to many other 'passenger' mutations that have no influence on phenotype. Yet evidence from fine mapping studies of individual quantitative trait loci in *S. cerevisiae* (Steinmetz et al., 2002) and metazoans (Mackay et al., 2009) alike suggest that multiple causal alleles can often occur within a single linked genetic locus. The increased phenotypic diversity that we observed in genetic crosses with

21

497 [*MPH1$^+$*] parents suggest, even in crosses with limited genetic diversity and in an organism with small

498 haplotype blocks, that alleles impacting the same phenotype can commonly be linked. This genetic

499 architecture may allow complex traits to persist in a greater number of meiotic progeny, which provides

500 theoretical adaptive advantages. But it also limits meiotic re-assortment of the linked alleles. The

501 [*MPH1$^+$*] prion provides a molecular mechanism through which this fundamental decision – whether to

502 couple or separate bits of genetic information as they are broadcast to the next generation – can be

503 reset. The phenotypic consequences of such re-assortment, at least in the context of traits relevant to

504 the clinical niche that we tested, are substantially more adaptive than would be expected from random

505 mutagenesis (where >95% of mutations are detrimental (Eyre-Walker and Keightley, 2007)).

506 Many prions have long been assumed to be non-functional assemblies of a homogenous

507 protein. However, the fact that the [*GAR$^+$*] prion is composed of multiple proteins (Jarosz et al., 2014)

508 suggests that some such elements might function as larger complexes. Indeed, the gain-of-function

509 phenotypes driven by [*MPH1$^+$*], as well as inheritance from one generation to the next, appear to be

510 dependent on other interacting DNA repair factors (especially those in the yeast FA pathway). Our data

511 also suggest that specific DNA structures may act act as important intermediates for [*MPH1$^+$*]

512 phenotypes. The linking of diverse physiological outcomes to a single epigenetic state suggests that

513 [*MPH1$^+$*] is a coordinated program that fuels specific and heritable changes in DNA repair networks.

514 During periods of nucleotide starvation, when cells are ill-suited to their environments, they can acquire

515 [*MPH1$^+$*] at higher rates. This improves their chances of survival and enhances phenotypic diversification

516 of the next generation. Mph1 is not alone in its capacity to assemble in response to replication fork

517 stress (Xue et al., 2014). Many DNA repair factors localize to large assemblies to exert their functions.

518 Our data provide an example in which such an assembly can encode a new set of activities that are

519 heritable over long biological timescales, with the capacity to permanently hardwire adaptive

520 phenotypic diversity into the genome.

Acknowledgements

Financial Interests Statement

The authors declare no competing financial interests.

534   **FIGURE LEGENDS**

535

536   **Figure 1. [*MPH1*$^+$] is a prion that protects against DNA damage mutagenesis.** (A) "Frequency of prion

537   infectivity" for protein transformation comparing [*mph1*$^-$] lysates (Mock) and [*MPH1*$^+$]-harboring lysates.

538   Infectivity is calculated as described in methods. [*MPH1*$^+$] was scored by resistance to ZnSO$_4$

539   (Chakrabortee et al., 2016). Infectivity from assembled [*PSI*$^+$] is displayed as a dotted horizontal line

540   (Tanaka and Weissman, 2006). (B) Growth of [*MPH1*$^+$] and *mph1*Δ cells in genotoxic stress relative to

541   naïve [*mph1*$^-$] cells. Error bars represent SEM from three or more biological replicates. (C-D)

542   Spontaneous and induced mutation frequencies of [*MPH1*$^+$] and *mph1*Δ cells, relative to naïve [*mph1*$^-$],

543   after growth in YPD (spontaneous) or after exposure to mutagenic agents (ex. 0.012% MMS or 100 μM

544   oxolinic acid) (see methods for details). Naïve mutation frequencies increased dramatically after

545   exposure to MMS and oxolinic acid (5×10^{-4} and 2×10^{-5} mutants per CFU respectively). Error bars

546   represent SEM from 3 independent experiments.

547

548   **Figure 2. [*MPH1*$^+$] requires helicase activity and FA pathway components.** (A) Experimental schema for

549   crossing [*MPH1*$^+$] into mutant strains to determine whether [*MPH1*$^+$]'s catalytic activity or interacting

550   proteins are required to manifest prion phenotypes (in haploid progeny) and/or propagate the prion. (B)

551   Haploid parents: growth of wild-type [*mph1*$^-$] and [*MPH1*$^+$] in the DNA damage stressor 4-NQO (1.2 μM).

552   Haploid mutant progeny: growth of [*mph1*$^-$] and [*MPH1*$^+$] strains harboring a single catalytically dead

553   point mutation (*mph1-Q603D)* in the *MPH1* gene in 1.2 μM 4-NQO. Heterozygous diploids: growth of

554   [*mph1*$^-$] and [*MPH1*$^+$] catalytically dead mutants in 1.2 μM 4-NQO after crossing back to a wild-type

555   strain. Error bars represent SEM determined from 6 biological replicates and are present on all plots. (C)

556   Left – Δ haploid: heatmap of Log2-transformed fold-changes in growth during DNA damage (4-NQO; see

557   methods) of haploid progeny harboring deletions of Mph1-associated proteins after crossing with an

558   [*MPH1*$^+$] strain. Data are normalized to isogenic [*mph1*$^-$] controls. Δ/WT diploid: data as above, but for

559   heterozygous diploids in which gene function was restored. Right – representative growth curves of

560   cross-back, heterozygous diploids in which the [*MPH1*⁺] phenotype was maintained or restored. Error

561   bars represent SEM determined from 6 biological replicates.

562

563   **Figure 3. Prion-like behavior and intrinsic disorder is conserved in human FANCM.** (A) Schematic

564   depicting the toxicity of casual protein overexpression in the presence of the corresponding prion. (B)

565   Growth of [*MPH1*⁺] strains harboring plasmids expressing FANCM and Mph1 variants. Values are

566   normalized to corresponding [*mph1*⁻] strains harboring the same plasmids. Error bars represent SEM

567   from six biological replicates. (C) Scores from an algorithm that predicts prion-like sequences using a

568   Hidden Markov model (PLAAC; (Lancaster et al., 2014)) for both Mph1 and Sup35. (D) Top: Intrinsic

569   disorder predictions (Disopred3; (Jones and Cozzetto, 2015)) for Mph1 and FANCM. Bottom: Variants

570   and domain architecture of Mph1 and FANCM used in this assay.

571

572   **Figure 4. [*MPH1*⁺] is a quasi-Lamarckian element.** (A) Diagram of spontaneous switching from [*mph1*⁻]

573   to [*MPH1*⁺]. In this experiment, naïve reporter cells were treated with indicated stressors for 12 hours

574   and assayed for modulated switching frequencies to [*MPH1*⁺]. (B) Induction of [*MPH1*⁺] compared to

575   control in various conditions. Error bars represent SEM from 3 biological replicates. (C) [*MPH1*⁺]-

576   dependent changes in mutation frequency following a transient *PIF1* overexpression to eliminate G-

577   quadruplex regions (Paeschke et al., 2013) and subsequent recovery after ~70 generations in rich media.

578   Values normalized to corresponding [*mph1*⁻] strain. Error bars represent SEM from 8 biological

579   replicates.

580

581   **Figure 5. [*MPH1*⁺] increases phenotypic diversification in the progeny of meiosis.** (A) Experimental

582   schema for measuring linkage between 2 auxotrophic markers in [*mph1*⁻] and [*MPH1*⁺] strains. (B)

25

583   Relative frequencies of His+ Ura+ meiotic recombinant progeny in [*mph1*⁻], [*MPH1*⁺], *mph1*Δ strains

584   compared to [*mph1*⁻]. Error bars represent SEM from 4 biological replicates. (C) Experimental schema for

585   determining [*MPH1*⁺]-dependent phenotypic diversification following a cross between lab strains (with

586   or without [*MPH1*⁺]) and a recently evolved clinical pathogen. (D-G) Histograms of normalized spore

587   colony sizes from these crosses (calculated using SGAtools (Wagih et al., 2013)) in 4 clinically relevant

588   stressors. Histograms were fit to a Gaussian distribution to generate curves.

589

590   **Supplemental Figure 1. Localization of Mph1 protein in [*MPH1*⁺] cells.** Fluorescence micrographs from

591   diploid cells harboring [*MPH1*⁺], or [*mph1*⁻] control, each expressing integrated *MPH1-YFP* from its

592   endogenous promoter. Exponential phased cells were imaged at OD_{600} ~0.5-0.8, stationary phase at

593   OD_{600} ~1.5-2.

594

595   **Supplemental Figure 2. [*MPH1*⁺] is a cytoplasmic element.** (A). Experimental schema of cytoduction

596   experiments. (B) Growth of [*mph1*⁻] and [*MPH1*⁺] cytoduced strains in a DNA stressor to which [*MPH1*⁺]

597   promotes resistance (10 µM mycophenolic acid). Error bars represent SEM from 3 biological replicates.

598   (C) Experimental schema for protein transformation experiments.

599

600   **Supplemental Figure 3. [*MPH1*⁺] does not influence GCR mutagenesis.** (A) Diagram of GCR reporter

601   used. Two counter-selectable markers (*URA3* and *CAN1*) are located upstream of an essential gene

602   (*PCM1*). When cells are presented with a double counter-selection, the probability of mutating both

603   genes in a single generation is vanishingly small. Therefore, resistant colonies will undergo a GCR event

604   at the precise location, preserving the essential gene. (B) GCR frequencies in [*mph1*⁻] and [*MPH1*⁺]

605   strains. Error bars represent SEM from 5 biological replicates.

606

607 **Supplemental Figure 4. [*MPH1*$^+$] increases homologous recombination**. Normalized genomic

608 integration frequencies of a linear DNA cassette in [*mph1*$^-$] and [*MPH1*$^+$] strains. Error bars represent

609 SEM for 6 biological replicates.

610

611 **Supplemental Figure 5. Expression levels of FANCM and Mph1 variants**. Bar graph showing the relative

612 expression levels of FANCM and Mph1 plasmids in [*MPH1*$^+$] vs. [*mph1*] strains measured using RT-PCR.

613 Error bars represent SEM from 3 biological replicates.

614

615 **Supplemental Figure 6. [*MPH1*$^+$] does not affect sporulation.** Fraction of tetrads in [*mph1*$^-$] and

616 [*MPH1*$^+$] strains after 5 days. Error bars represent SEM from 3 biological replicates.

617

618 **Supplemental Figure 7. Phenotypic variation in [*mph1*$^-$] and [*MPH1*$^+$] derivatives of laboratory and**

619 **clinical parent strains.** Phenotypic distributions of [*mph1*$^-$] or [*MPH1*$^+$] parental strains for wild cross in

620 the 4 different stressors. Range of x-axis used is identical to each corresponding progeny histogram in

621 Figure 5.

622

623 **Supplemental Figure 8. Mph1 does not act as a phenotypic capacitor.** Top panel: [*MPH1*$^+$] parent strain

624 before and after prion 'curing' spotted in a 10-fold dilution series on a plate containing 10 mM ZnSO$_4$.

625 Bottom panel: Heat-resistant progeny from wild outcross with an [*MPH1*$^+$] parent before and after prion

626 'curing' spotted in a 10-fold dilution series on a YPD plate grown at 39 °C.

627

628 **Supplemental Table 1. Yeast strains used in this study.**

629

630 **Supplemental Table 2. Plasmids used in this study.**

631

632 **Supplemental Table 3. Interacting proteins required for [$MPH1^+$]-dependent anti-mutator phenotypes**.

633 Table showing [$mph1^-$] and [$MPH1^+$] mutation frequencies for haploid progeny harboring genetic

634 knockouts of DNA repair factors. 1st column – genotypes of each strain assayed; 2nd column – mutation

635 frequency with SEM for each knockout in a naïve [$mph1^-$] strain; 3rd column – mutation frequency with

636 SEM for corresponding [$MPH1^+$] strain; 4th column – Fold-change in mutation frequency by each genetic

637 knockout compared to a wild-type naïve [$mph1^-$] strain; 5th column – Fold-change in mutation frequency

638 imparted by [$MPH1^+$] for the same genotype.

639

640 **REFERENCES**

641 Alter, B.P. (1996). Fanconi's anemia and malignancies. Am J Hematol *53*, 99-110.

642 Audas, T.E., Audas, D.E., Jacob, M.D., Ho, J.J., Khacho, M., Wang, M., Perera, J.K., Gardiner, C., Bennett,

643 C.A., Head, T*., et al.* (2016). Adaptation to Stressors by Systemic Protein Amyloidogenesis. Dev Cell *39*,

644 155-168.

645 Banerjee, S., Smith, S., Oum, J.H., Liaw, H.J., Hwang, J.Y., Sikdar, N., Motegi, A., Lee, S.E., and Myung, K.

646 (2008). Mph1p promotes gross chromosomal rearrangement through partial inhibition of homologous

647 recombination. J Cell Biol *181*, 1083-1093.

648 Cerami, E., Gao, J., Dogrusoz, U., Gross, B.E., Sumer, S.O., Aksoy, B.A., Jacobsen, A., Byrne, C.J., Heuer,

649 M.L., Larsson, E*., et al.* (2012). The cBio cancer genomics portal: an open platform for exploring

650 multidimensional cancer genomics data. Cancer Discov *2*, 401-404.

651 Chakrabortee, S., Byers, J.S., Jones, S., Garcia, D.M., Bhullar, B., Chang, A., She, R., Lee, L., Fremin, B.,

652 Lindquist, S*., et al.* (2016). Intrinsically Disordered Proteins Drive Emergence and Inheritance of

653 Biological Traits. Cell *167*, 369-381 e312.

654 Chen, Y.H., Choi, K., Szakal, B., Arenz, J., Duan, X., Ye, H., Branzei, D., and Zhao, X. (2009). Interplay

655 between the Smc5/6 complex and the Mph1 helicase in recombinational repair. Proc Natl Acad Sci U S A

656 *106*, 21252-21257.

657 Crismani, W., Girard, C., Froger, N., Pradillo, M., Santos, J.L., Chelysheva, L., Copenhaver, G.P., Horlow,

658 C., and Mercier, R. (2012). FANCM limits meiotic crossovers. Science *336*, 1588-1590.

659 Daee, D.L., Ferrari, E., Longerich, S., Zheng, X.F., Xue, X., Branzei, D., Sung, P., and Myung, K. (2012).

660 Rad5-dependent DNA repair functions of the Saccharomyces cerevisiae FANCM protein homolog Mph1.

661 J Biol Chem *287*, 26563-26575.

662 Derkatch, I.L., Bradley, M.E., Hong, J.Y., and Liebman, S.W. (2001). Prions affect the appearance of other

663 prions: the story of [PIN(+)]. Cell *106*, 171-182.

664 Douglas, P.M., Treusch, S., Ren, H.Y., Halfmann, R., Duennwald, M.L., Lindquist, S., and Cyr, D.M. (2008).

665 Chaperone-dependent amyloid assembly protects cells from prion toxicity. Proc Natl Acad Sci U S A *105*,

666 7206-7211.

667 Eyre-Walker, A., and Keightley, P.D. (2007). The distribution of fitness effects of new mutations. Nat Rev

668 Genet *8*, 610-618.

669 Farmer, S., San-Segundo, P.A., and Aragon, L. (2011). The Smc5-Smc6 complex is required to remove

670 chromosome junctions in meiosis. PloS one *6*, e20948.

671 Fricke, W.M., and Brill, S.J. (2003). Slx1-Slx4 is a second structure-specific endonuclease functionally

672 redundant with Sgs1-Top3. Genes Dev *17*, 1768-1778.

673 Gietz, D., St Jean, A., Woods, R.A., and Schiestl, R.H. (1992). Improved method for high efficiency

674 transformation of intact yeast cells. Nucleic Acids Res *20*, 1425.

675 Halfmann, R., Alberti, S., and Lindquist, S. (2010). Prions, protein homeostasis, and phenotypic diversity.

676 Trends Cell Biol *20*, 125-133.

677   Holmes, D.L., Lancaster, A.K., Lindquist, S., and Halfmann, R. (2013). Heritable remodeling of yeast

678   multicellularity by an environmentally responsive prion. Cell *153*, 153-165.

679   Huang, J., Liu, S., Bellani, M.A., Thazhathveetil, A.K., Ling, C., de Winter, J.P., Wang, Y., Wang, W., and

680   Seidman, M.M. (2013). The DNA translocase FANCM/MHF promotes replication traverse of DNA

681   interstrand crosslinks. Mol Cell *52*, 434-446.

682   Jarosz, D.F., Brown, J.C., Walker, G.A., Datta, M.S., Ung, W.L., Lancaster, A.K., Rotem, A., Chang, A.,

683   Newby, G.A., Weitz, D.A.*, et al.* (2014). Cross-kingdom chemical communication drives a heritable,

684   mutually beneficial prion-based transformation of metabolism. Cell *158*, 1083-1093.

685   Jarosz, D.F., Taipale, M., and Lindquist, S. (2010). Protein homeostasis and the phenotypic manifestation

686   of genetic diversity: principles and mechanisms. Annu Rev Genet *44*, 189-216.

687   Jones, D.T., and Cozzetto, D. (2015). DISOPRED3: precise disordered region predictions with annotated

688   protein-binding activity. Bioinformatics *31*, 857-863.

689   Kulak, N.A., Pichler, G., Paron, I., Nagaraj, N., and Mann, M. (2014). Minimal, encapsulated proteomic-

690   sample processing applied to copy-number estimation in eukaryotic cells. Nat Methods *11*, 319-324.

691   Lancaster, A.K., and Masel, J. (2009). The evolution of reversible switches in the presence of irreversible

692   mimics. Evolution *63*, 2350-2362.

693   Lancaster, A.K., Nutter-Upham, A., Lindquist, S., and King, O.D. (2014). PLAAC: a web and command-line

694   application to identify proteins with prion-like amino acid composition. Bioinformatics *30*, 2501-2502.

695   Lorenz, A., Osman, F., Sun, W., Nandi, S., Steinacher, R., and Whitby, M.C. (2012). The fission yeast

696   FANCM ortholog directs non-crossover recombination during meiosis. Science *336*, 1585-1588.

697   Mackay, T.F., Stone, E.A., and Ayroles, J.F. (2009). The genetics of quantitative traits: challenges and

698   prospects. Nat Rev Genet *10*, 565-577.

699   McMahill, M.S., Sham, C.W., and Bishop, D.K. (2007). Synthesis-dependent strand annealing in meiosis.

700   PLoS Biol *5*, e299.

701   Meetei, A.R., Sechi, S., Wallisch, M., Yang, D., Young, M.K., Joenje, H., Hoatlin, M.E., and Wang, W.

702   (2003). A multiprotein nuclear complex connects Fanconi anemia and Bloom syndrome. Mol Cell Biol *23*,

703   3417-3426.

704   Moldovan, G.L., and D'Andrea, A.D. (2009). How the fanconi anemia pathway guards the genome. Annu

705   Rev Genet *43*, 223-249.

706   Paeschke, K., Bochman, M.L., Garcia, P.D., Cejka, P., Friedman, K.L., Kowalczykowski, S.C., and Zakian,

707   V.A. (2013). Pif1 family helicases suppress genome instability at G-quadruplex motifs. Nature *497*, 458-

708   462.

709   Rockmill, B., Lambie, E.J., and Roeder, G.S. (1991). Spore enrichment. Methods in Enzymology *194*, 146-

710   149.

711   Scheller, J., Schurer, A., Rudolph, C., Hettwer, S., and Kramer, W. (2000). MPH1, a yeast gene encoding a

712   DEAH protein, plays a role in protection of the genome from spontaneous and chemically induced

713   damage. Genetics *155*, 1069-1081.

714   Shorter, J., and Lindquist, S. (2005). Prions as adaptive conduits of memory and inheritance. Nat Rev

715   Genet *6*, 435-450.

716   Soustelle, C., Vedel, M., Kolodner, R., and Nicolas, A. (2002). Replication protein A is required for meiotic

717   recombination in Saccharomyces cerevisiae. Genetics *161*, 535-547.

718   Steinmetz, L.M., Sinha, H., Richards, D.R., Spiegelman, J.I., Oefner, P.J., McCusker, J.H., and Davis, R.W.

719   (2002). Dissecting the architecture of a quantitative trait locus in yeast. Nature *416*, 326-330.

720   Strope, P.K., Skelly, D.A., Kozmin, S.G., Mahadevan, G., Stone, E.A., Magwene, P.M., Dietrich, F.S., and

721   McCusker, J.H. (2015). The 100-genomes strains, an S. cerevisiae resource that illuminates its natural

722   phenotypic and genotypic variation and emergence as an opportunistic pathogen. Genome Res *25*, 762-

723   774.

724   Suzuki, G., Shimazu, N., and Tanaka, M. (2012). A yeast prion, Mod5, promotes acquired drug resistance

725   and cell survival under environmental stress. Science *336*, 355-359.

726   Tanaka, M., and Weissman, J.S. (2006). An efficient protein transformation protocol for introducing

727   prions into yeast. Methods Enzymol *412*, 185-200.

728   True, H.L., and Lindquist, S.L. (2000). A yeast prion provides a mechanism for genetic variation and

729   phenotypic diversity. Nature *407*, 477-483.

730   Wagih, O., Usaj, M., Baryshnikova, A., VanderSluis, B., Kuzmin, E., Costanzo, M., Myers, C.L., Andrews,

731   B.J., Boone, C.M., and Parts, L. (2013). SGAtools: one-stop analysis and visualization of array-based

732   genetic interaction screens. Nucleic Acids Res *41*, W591-596.

733   Ward, T.A., Dudasova, Z., Sarkar, S., Bhide, M.R., Vlasakova, D., Chovanec, M., and McHugh, P.J. (2012).

734   Components of a Fanconi-like pathway control Pso2-independent DNA interstrand crosslink repair in

735   yeast. PLoS genetics *8*, e1002884.

736   Whitby, M.C. (2010). The FANCM family of DNA helicases/translocases. DNA Repair (Amst) *9*, 224-236.

737   Wickner, R.B., Edskes, H.K., and Shewmaker, F. (2006). How to find a prion: [URE3], [PSI+] and [beta].

738   Methods *39*, 3-8.

739   Xue, X., Choi, K., Bonner, J., Chiba, T., Kwon, Y., Xu, Y., Sanchez, H., Wyman, C., Niu, H., Zhao, X.*, et al.*

740   (2014). Restriction of replication fork regression activities by a conserved SMC complex. Molecular cell

741   *56*, 436-445.

742   Xue, X., Choi, K., Bonner, J.N., Szakal, B., Chen, Y.H., Papusha, A., Saro, D., Niu, H., Ira, G., Branzei, D.*, et*

743   *al.* (2015a). Selective modulation of the functions of a conserved DNA motor by a histone fold complex.

744   Genes Dev *29*, 1000-1005.

745   Xue, X., Sung, P., and Zhao, X. (2015b). Functions and regulation of the multitasking FANCM family of

746   DNA motor proteins. Genes Dev *29*, 1777-1788.

747   Young, C.W., Schochetman, G., and Karnofsky, D.A. (1967). Hydroxyurea-induced inhibition of

748   deoxyribonucleotide synthesis: studies in intact cells. Cancer Res *27*, 526-534.

749

Figure 1

A

Frequency of prion infectivity

B

Growth in Genotoxic Stressors

C

Canavanine Mutagenesis

D

Fluconazole mutagenesis

Figure 2

A

B

[*MPH1*⁺] catalytic requirement

C

Figure 3

A

[*prion⁻*] cells   [*PRION⁺*] cells

Overexpress casual protein

Overexpress casual protein

Normal growth   Impaired growth

B

Prion-dependent toxicity of overexpression

Growth of [*MPH1⁺*]/ [*mph1⁻*]

Mph1   Mph1ΔC   FANCM   FANCMΔC

Expressed protein

C

Prion Sequence Score

Score

Mph1
Sup35

Amino Acid

D

Mph1 Disorder Probability

Score

Amino Acid

FANCM Disorder Probability

Score

Amino Acid

Variants:

ScMph1   Helicase   Regulatory   1 ... 993

ScMph1ΔC   Helicase   1 ... 753

Variants:

hsFANCM   Helicase   Reg.   Nuclease   1 ... 2048

hsFANCMΔC   Helicase   1 ... 695

Figure 4

Figure 5

Figure S1

Exponential phase

Stationary phase

Figure S2

Figure S3

A

Counter-selectable markers   Essential gene

URA3   CAN1   PCM1

↓ GCR event

Canavanine, 5-FOA resistant

PCM1

B

GCR mutagenesis

n.s.

Frequency

10^{-6}

10^{-7}

10^{-8}

10^{-9}

[$mph1^-$]   [$MPH1^+$]

Figure S4

Homologous Recombination

Figure S5

Mph1/FANCM Expression

Figure S6

Sporulation efficiency

n.s.

Figure S7

Lab parents

39°C Lab Parents

$F=2.219$
$p=0.062$

[mph1-] lab parent
[MPH1+] lab parent

Fluconazole Lab Parents

$F=1.284$
$p=0.529$

[mph1-] lab parent
[MPH1+] lab parent

Amphotericin B Lab Parents

$F=2.254$
$p=0.174$

[mph1-] lab parent
[MPH1+] lab parent

H₂O₂ Lab Parents

$F=1.775$
$p=0.335$

[mph1-] lab parent
[MPH1+] lab parent

Clinical parents

39°C Clinical Parents

$F=6.400$
$p=0.001$

[mph1-] clinical parent
[MPH1+] clinical parent

Fluconazole Clinical Parents

$F=3.158$
$p=0.004$

[mph1-] clinical parent
[MPH1+] clinical parent

Amphotericin B Clinical Parents

$F=1.966$
$p=0.256$

[mph1-] clinical parent
[MPH1+] clinical parent

H₂O₂ Clinical Parents

$F=1.829$
$p=0.309$

[mph1-] clinical parent
[MPH1+] clinical parent

Figure S8

10-fold dilution series

[*MPH1*+]
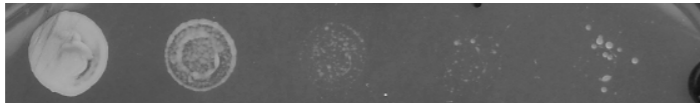
[*MPH1*+] "cured"

10mM ZnSO$_4$
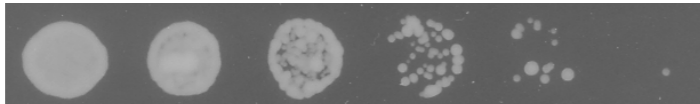
[*MPH1*+] meiotic progeny

[*MPH1*+] meiotic progeny "cured"

39ºC Heat Stress

Table S1
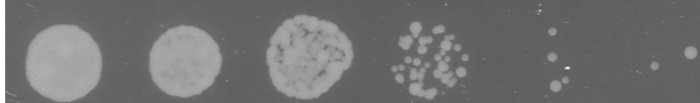
Strain	Source
mph1-Q603D-3Flag::HIS3	Xiaolan Zhao lab (MSKCC)
BY4742 rad5Δ	Yeast MATα deletion library
BY4742 rad51Δ	Yeast MATα deletion library
BY4742 sgs1Δ	Yeast MATα deletion library
BY4742 srs2Δ	Yeast MATα deletion library
BY4742 mhf1Δ	Yeast MATα deletion library
BY4742 mhf2Δ	Yeast MATα deletion library
BY4742 chl1Δ	Yeast MATα deletion library
BY4742 exo1Δ	Yeast MATα deletion library
BY4742 mgm101Δ	Yeast MATα deletion library
BY4742 msh2Δ	Yeast MATα deletion library
BY4742 msh6Δ	Yeast MATα deletion library
BY4742 pso2Δ	Yeast MATα deletion library
BY4742 slx4Δ	Yeast MATα deletion library
BY4741 mph1Δ	Yeast MATα deletion library
YJM975	SGRP collection
Mph1-YFP	Xiaolan Zhao lab (MSKCC)
MDG1::K.lactisURA3 prion reporter	Chakrabortee et al., 2016

Table S2

Plasmid	Source
pUG72	Euroscarf
416-GPD-ccdB-eGFP	Addgene Yeast Gateway kit
416-GPD-Mph1-eGFP	Addgene Yeast Gateway kit; Yeast ORFeome collection E. coli (YSC3868)
416-GPD-Mph1ΔC-eGFP	Addgene Yeast Gateway kit; Yeast ORFeome collection E. coli (YSC3868)
416-GPD-FANCM-eGFP	Addgene Yeast Gateway kit; FANCM from Stephen West lab
416-GPD-FANCMΔC-eGFP	Addgene Yeast Gateway kit; GE Life Sciences Human ORFeome library
Hsp70(K69M)	Jarosz et al., 2014b

Table S3

Genotype	[*mph1⁻*] Mutation frequency	[*MPH1⁺*] Mutation frequency	Mutation fold change by genotype	Mutation fold change by prion
wild-type	3.33(±1.31)x10^(-8)	8.89(±4.44)x10^(-9)		0.3
rad5Δ	9.16(±4.89)x10^(-7)	9.69(±3.98)x10^(-7)	27.5	1.1
rad51Δ	1.99(±0.36)x10^(-6)	1.10(±0.25)x10^(-6)	59.6	0.6
sgs1Δ	2.50(±0.69)x10^(-8)	9.28(±3.67)x10^(-8)	0.8	3.7
srs2Δ	3.40(±1.06)x10^(-8)	5.67(±0.78)x10^(-8)	1.0	1.7
mhf1Δ	1.17(±0.35)x10^(-7)	1.00(±0.22)x10^(-7)	3.5	0.9
mhf2Δ	7.50(±2.17)x10^(-8)	3.00(±1.22)x10^(-7)	2.3	4.0
chl1Δ	2.53(±0.37)x10^(-7)	4.06(±1.15)x10^(-7)	7.6	1.6
exo1Δ	1.14(±0.13)x10^(-6)	1.36(±0.12)x10^(-6)	34.1	1.2
mgm101Δ	3.62(±2.24)x10^(-7)	2.50(±1.52)x10^(-8)	10.9	0.1
msh2Δ	3.18(±0.18)x10^(-6)	3.14(±0.19)x10^(-6)	95.3	1.0
msh6Δ	1.73(±0.20)x10^(-6)	1.62(±0.09)x10^(-6)	51.9	0.9
pso2Δ	3.89(±0.98)x10^(-7)	1.78(±0.04)x10^(-7)	11.7	0.5
slx4Δ	7.92(±1.62)x10^(-8)	8.89(±4.76)x10^(-7)	2.4	11.2